J. Fluid Mech. (1997), *vol.* 352, *pp.* 283–303. Printed in the United Kingdom

The anomalous wake accompanying bubbles rising in a thin gap: a mechanically forced Marangoni flow

By JOHN W. M. BUSH

Department of Applied Mathematics and Theoretical Physics, University of Cambridge, Silver Street, Cambridge CB3 9EW, UK

(Received 30 October 1996 and in revised form 12 May 1997)

A novel wake structure, observed as penny-shaped air bubbles rise at moderate Reynolds number through a thin layer of water bound between parallel glass plates inclined at a shallow angle relative to the horizontal, is reported. The structure of the wake is revealed through tracking particles suspended in the water. The wake completely encircles the rising bubble, and is characterized by a reverse surface flow or 'edge jet' which transports fluid in a thin boundary layer along the bubble surface from the tail to the nose at speeds which are typically an order of magnitude larger than the bubble rise speed. A consistent physical explanation for the wake structure is proposed. The wake is revealed to be a manifestation of the three-dimensionality of the flow in the suspending fluid. The bubble surface advances through a rolling motion, thus generating regions of surface divergence and convergence at, respectively, the leading and trailing edges of the bubble. A nose-to-tail gradient in surfactant concentration is thus established, and the associated surface tension gradient drives the edge jet. The dependence of the wake structure on the suspending fluid is examined experimentally.

Surfactants play an anomalous role in the reported flow, serving to promote rather than suppress surface motions. The wake structure is an example of a mechanically forced Marangoni flow, and so represents a mechanical analogue of that accompanying thermocapillary drop motion in microgravity. A theoretical model is developed which reproduces the salient features of the flow, and on the basis of which an estimate is made of the mechanically induced surface tension gradient along the bubble surface.

1. Introduction

Surface-active agents, or surfactants, are molecules in solution that find it energetically favourable to reside on liquid–gas or liquid–liquid interfaces. Once in place on the surface, they serve to decrease the interfacial tension; consequently, surface motions which generate gradients in surfactant material are resisted by an effective surface elasticity. The ability of surfactants to influence the dynamics of drops and bubbles has been known for some time (e.g. Levich 1962; Harper 1972). For both high- and low-Reynolds-number bubble motions, advection causes surfactant to accumulate at the rear stagnation point of the bubble, giving rise to a surfactant gradient from nose to tail. The associated surface stress opposes the surface motion, thus immobilizing or 'rigidifying' the bubble surface and giving rise to steady rise speeds which are significantly less than those predicted theoretically. When the surfactant

gradients are established in this manner, they must act to resist the surface flow and cannot act to reverse its direction. In this paper, we present an example where surfactant gradients established on the bubble surface do not play their usual role in resisting the surface flow, but, conversely, drive vigorous motions in a direction opposed to the free stream.

The problem of bubble motion in a Hele-Shaw cell, a thin gap in which fluid motions are viscously dominated, has been considered in some detail (e.g. Maxworthy 1986), and the influence of surfactants on the bubble shapes and steady rise speeds has been examined by Park, Maruvada & Yoon (1994). The influence of thermally induced surface tension gradients on a drop in a Hele-Shaw cell has recently been considered by Nadim, Borhan & Haj-Hariri (1996) and Boos & Thess (1997). The problem of moderate-Reynolds-number bubble motion in a thin gap has received relatively little attention. Siekmann, Eck & Johann (1974) performed an experimental study that spanned a broad range of Reynolds numbers and observed a myriad of bubble forms, but were concerned exclusively with the shapes and rise speeds of the bubbles and so did not measure the form of the flow in the suspending fluid. In a recent experimental study, Bush & Eames (1998) examined the fluid displacement associated with high-Reynolds-number bubble motion in a thin gap by tracking neutrally buoyant particles suspended in the fluid. The same experimental technique has been employed here in order to examine this moderate-Reynolds-number phenomenon.

Consider a penny-shaped air bubble of characteristic radius a rising at a speed U through water bound in a thin gap of thickness d with a characteristic Reynolds number $Re = Ua/\nu$. When the gap is inclined at a very shallow angle relative to the horizontal so that $1 < Re(d/a)^2 < 50$ and $d/a \ll 1$, a peculiar wake structure is observed to accompany the bubble. The wake structure, henceforth referred to as 'anomalous', is characterized by two salient features (refer to figure 1). First, the wake completely encircles the bubble, so that the fluid within the bounding wake streamline, or separatrix, is transported with the bubble. The leading edge of the encircling wake will henceforth be referred to as an 'upstream disturbance'. Second, there is an intense boundary layer flow adjoining the bubble surface, henceforth referred to as the 'edge jet', which transports fluid from the tail of the bubble to the nose at speeds exceeding the bubble rise speed.

In §2, we present the results of an experimental study in which we detail the variation of the wake structure with increasing Reynolds number and demonstrate the sensitivity of the wake structure to the properties of the suspending fluid. In §3, we propose a physical explanation for the observed flow structure which is consistent with the experimental observations. In §4, we present the equations governing the dynamics of the suspending fluid and the bubble surface. In §5, we present a theoretical model of Marangoni bubble motion in a Hele-Shaw cell which reproduces the salient features of the observed flow. The similarities between the reported flow and those arising in a number of thermocapillary drop motions are discussed in §6.

2. Experimental observations

The anomalous flow structure was first observed in a simple device consisting of a thin ($\sim$ 2 mm) gap of water bound between two rectangular glass plates glued together at their edges. Provided a volume of air is contained within the gap, and Pearlescence (or Kalliroscope) is suspended in the water, one may readily observe a variety of bubble shapes and flow forms characteristic of moderate- and high-Reynolds-number bubble motion in two dimensions. Moreover, when the gap is

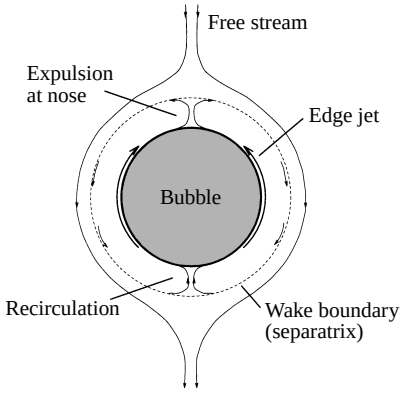

FIGURE 1. The peculiar wake structure observed at moderate Reynolds number, as viewed in the frame of reference translating uniformly with the bubble. Note the presence of four stagnation points in the flow. The wake entirely encircles the bubble, and is characterized by an intense 'edge jet' which transports fluid from the tail to the nose and may lead to a 'reverse separation' on the bubble's leading edge.

inclined at very shallow angles (1°–2°) relative to the horizontal, one may observe the anomalous wake structure to be considered here. A number of such thin-gap devices (with either glass or Plexiglas bounding plates) were used to make qualitative observations; however, quantitative measurements required a series of experiments in a more elaborate apparatus.

Two 12 mm thick glass plates, of dimension 46 cm by 86 cm, were clamped together and separated by a margin of rubber spacer of thickness 2.5 mm. The system was mounted on a frame, and inclined at a shallow angle α relative to the horizontal. The thin gap was filled with the desired fluid, either an aqueous solution or a silicone oil, along with white plyolite particles (of diameter 250 μm) which were clearly visible against the lower plate of black glass. Air bubbles were introduced into the suspending fluid through a syringe attached to a one-way valve inlet at the base of the gap. The form of the flow induced in the suspending fluid could be deduced by tracking the plyolite particles with the DigImage system (Dalziel 1992). On a number of occasions, the motion of the bubble surface was visualized by injecting a fine suspension of lycopodium powder with the bubble.

Figure 2 illustrates the particle paths observed around an air bubble rising through saltwater, and indicates the two salient flow features highlighted in figure 1. Particles are transported in the edge jet from the tail to the nose along the bubble surface, ejected at the bubble nose, then swept back towards its rear, where they are re-entrained into the edge jet. Particles are recycled within the separatrix which defines the boundary of the wake, and so are transported bodily with the bubble. The velocities of the particles in the edge jet are typically an order of magnitude larger than the rise speed of the bubble. The thickness of the edge jet is comparable to the gap thickness, and so is small relative to the bubble radius.

Figure 3 illustrates qualitatively the variation of the wake structure with increasing $Re(d/a)^2$, an evolution which is detailed by the data presented in figure 4. The boundaries of the wake are defined by stagnation points at distances δ_1 and δ_2, respectively up- and downstream of the bubble. For $Re(d/a)^2 < 5$, the wake encircles the bubble, and is roughly circular. As $Re(d/a)^2$ increases beyond 20, the wake becomes progressively less pronounced upstream of the bubble; moreover, it becomes

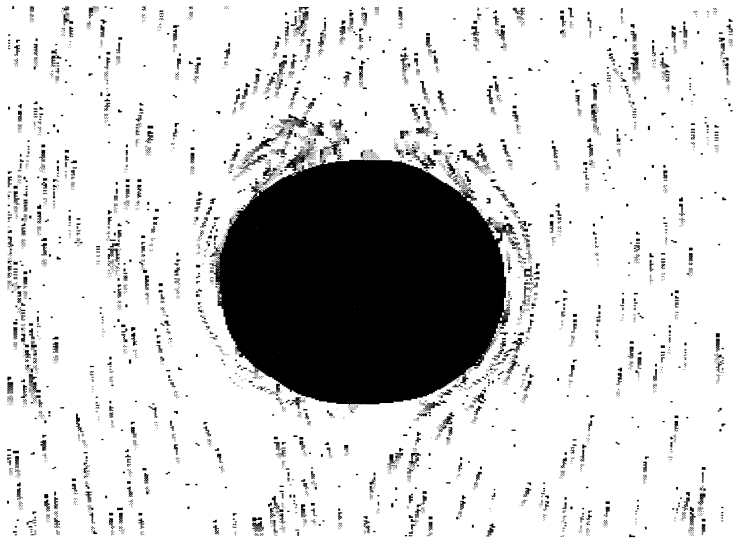

FIGURE 2. Particle paths observed around an oblate air bubble of half-width 3.2 cm which rose uniformly (with gap Reynolds number of 5) through a 2.5 mm gap of 3.2% saltwater solution bound between glass plates inclined at 1.3° relative to the horizontal. The particle tracking was done in the frame of reference of the bubble, so that particles upstream of (above) the bubble appear to stream towards the bubble. Note the region of intense reverse flow (the edge jet) adjoining the bubble surface which transports particles from the tail to the nose of the bubble.

oval, elongated in the direction of motion. The wake centre no longer coincides with the bubble centre, but is shifted slightly downstream. This offset of the wake and bubble centres and the wake elongation become more pronounced as the Reynolds number increases, until finally the leading edge of the oval wake coincides with the leading edge of the bubble. For $Re(d/a)^2 > 60$, the wake is entirely confined to the rear region of the bubble. Throughout this progression, the bubbles assume oblate elliptical shapes whose height $2b$ to width $2a$ ratio decreases from 1 to 0.6.

In a number of experiments, a small amount of lycopodium powder was injected with the air bubble. The powder quickly settled onto the bubble surface, and so made it possible to observe the motions at the air–water boundary. The form of the motion on the bubble surface is illustrated schematically in figure 5. Particles starting at the front edge of the bubble are rolled onto the bounding walls where they remain until the rear edge of the bubble reaches them. They are then rolled onto the rear edge of the bubble, and swept at high speed along the side edge until they reach the front of the bubble, where they are again rolled onto the surface. Note that the lycopodium particles never leave the bubble surface, and so behave like surfactants. Moreover, particles initially on the channel walls which are overrun by the bubble become trapped on the bubble surface and are subsequently transported with the bubble.

If the bubble surface behaves like a material surface, the areas being rolled onto and off the channel walls at, respectively, the leading and trailing edges of the bubble would be equal to the areal flux along the edge of the bubble:

$$2Ua \sim \pi U_j d \tag{2.1}$$

where U_j is the characteristic edge jet speed, and we assume that the bubble edges are semicircular in cross-section. Figure 6 indicates that the observed edge-jet speeds are

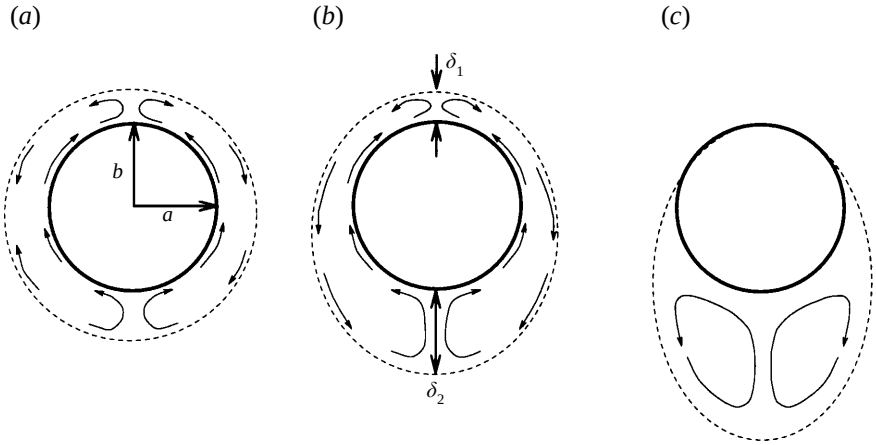

FIGURE 3. A schematic illustration indicating the effect of increasing Reynolds number on the anomalous wake structure. At the lowest Reynolds numbers observed (*a*), the wake is to a good approximation fore-aft symmetric, and entirely encircles the bubble. As *Re* increases, the fore-aft symmetry is broken (*b*), and the wake is swept to the rear of the bubble, eventually taking the form typically expected at high *Re* (*c*).

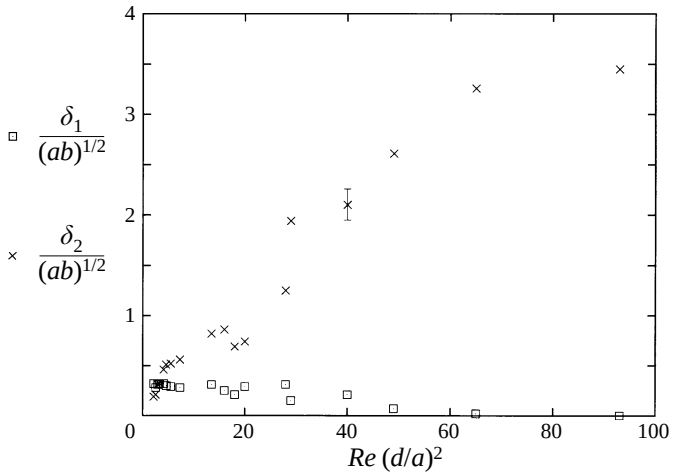

FIGURE 4. The observed dependence of wake shape on gap Reynolds number, $Re(d/a)^2$, for air bubbles rising through a 3.2% saltwater solution bound in a 2.5 mm gap inclined at 2° relative to the horizontal. □ and × denote the non-dimensional wake thicknesses at the leading and trailing edges of the bubble, respectively, $\delta_1/(ab)^{1/2}$ and $\delta_2/(ab)^{1/2}$, where *a* and *b* denote the half-width and half-height of the bubble.

roughly consistent with (2.1) and so with the physical picture of the bubble surface behaving as a material surface: fluid elements initially on the bubble surface remain there indefinitely.

Figure 7 summarizes the observations of the flows generated by bubble or rigid particle motion in a thin gap; specifically, it indicates the conditions under which upstream disturbances and edge jets were observed. The upstream disturbance accompanies bubbles rising through aqueous solutions as well as translating rigid particles (in particular, a penny) sliding in contact with the channel walls. The upstream disturbance was not evident in the silicone oils when the gap width was 2.5 mm.

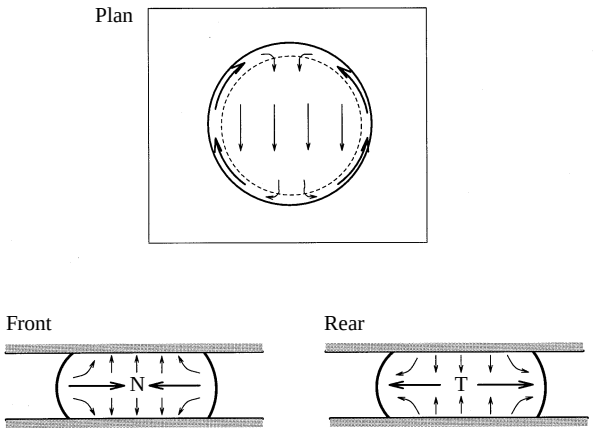

FIGURE 5. A schematic illustration of the surface velocity field observed on an air bubble rising through a thin gap of water, revealed using a fine lycopodium powder which settled on the bubble surface. The bubble surface moves through a rolling motion. The distance between the plates is greatly exaggerated for the sake of clarity. The dashed line in the plan view corresponds to the air–water–glass contact line. Note the stagnation points at the nose (N) and tail (T) of the bubble.

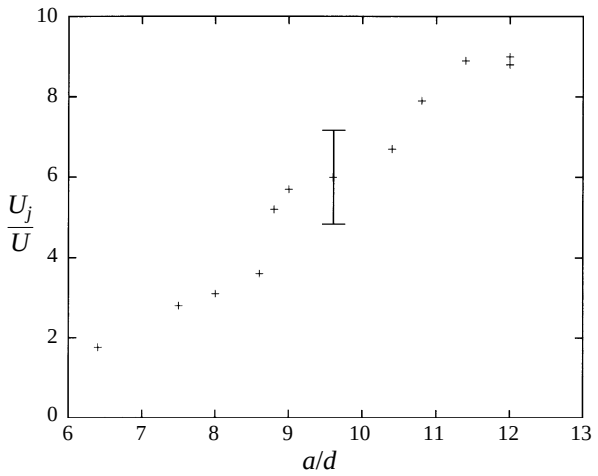

FIGURE 6. The observed dependence of the maximum observed edge-jet speed on the bubble size for bubbles rising along a 1.3° incline through a 3.2% saltwater solution. A representative error bar is shown.

Changing the bounding plates from glass to Plexiglas had no appreciable impact on the form of the flow. The anomalous wake structure was most pronounced when the suspending fluid was saltwater, and the intensity of the edge jet appeared to increase progressively with salt concentration over the range of concentrations considered. The edge jet vanished in all of the silicone oils considered. When significant amounts of either soap or wetting agent were added to the aqueous solution, the intensity of the edge jet was diminished. When concentrated wetting agent, Ilfotol, was used as the suspending fluid, the edge jet was completely suppressed.

Our experimental study was limited in that we were not able to readily resolve the details of the flow in the immediate vicinity of the bounding plates. Nonetheless, it was possible to observe whether or not the suspending fluid was wetting the bounding

Configuration	Upstream disturbance	Edge jet
Air H_2O	Y	Y
Penny H_2O, Si	Y	N
Air Si	N	N
Air Ilfotol	N	N

FIGURE 7. Table indicating when upstream disturbances and edge jets were observed in a number of cases of bubble and particle motion in a thin gap. Si denotes silicone oil (a variety of which were used, with viscosities ranging between 1 and 1000 cS). Ilfotol is a wetting agent. Changing the bounding material from glass to Plexiglas did not have a significant impact on the wake structure. The anomalous wake structure was most pronounced when the suspending fluid was saltwater.

channel: the channel walls were partially wet by the aqueous solutions considered, and fully wet by the silicone oils. It was also impossible to identify the various surfactants in our system, or to measure their concentrations. Finally, we were unable to see what form the flow would take under 'hyperclean' conditions, as might arise if the bubble were rising through triply distilled water bound between specially treated glass.

3. Physical explanation

Figure 8 is a sketch which describes qualitatively the fluid motion in a plane perpendicular to the bounding plates and coincident with the centreline of the bubble. It illustrates the flow accompanying bubble motion through water, which partially wets the glass, so that a corner exists. In accordance with the observations reported in figure 5, the bubble surface advances through a rolling motion. The fluid adjoining the channel walls is dragged into the leading edge of the bubble, and so must be either swept around the edge of the bubble or ejected radially. Similarly, at the trailing edge of the bubble, fluid in the viscous boundary layer is drawn away from the corner by the moving wall, and so must be replaced by fluid drawn in from the interior. The flow structure in the neighbourhood of the corners may thus resemble that arising when a meniscus between two viscous fluids advances along the length of a circular capillary tube (Dussan V. 1977); however, the three-dimensionality of the flow and the dynamic influence of fluid inertia introduce added complexity.

The presence of an upstream disturbance may thus be simply understood through consideration of the interaction between the viscous boundary layers adjoining the channel walls and the advancing bubble. The fact that it also accompanies a sliding penny indicates that it is a generic feature of particle motion in a thin gap. The extent of the upstream disturbance will generally depend on the wetting properties of the fluid, and so on both the capillary number $Ca = \rho\nu U/\sigma$ based on the interfacial tension σ, and the surfactant distribution (Ratulowski & Chang 1990). The upstream disturbance is most pronounced when the suspending fluid is either non- or partially wetting, in which case well-defined corners exist along the bubble margins and most

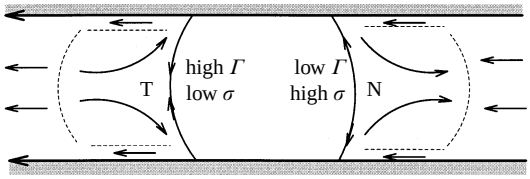

FIGURE 8. A schematic illustration of the three-dimensional flow induced by an air bubble rising through an aqueous solution bound between two plates, as viewed in the bubble frame of reference in a plane coincident with the bubble's centreline. The distance between the plates is greatly exaggerated for clarity. The rolling bubble surface leads to an excess of surfactant at the trailing edge, and a deficit at the leading edge. The associated azimuthal surface tension gradient drives the edge jet illustrated in figure 1.

efficiently displace fluid from the channel walls. When the suspending fluid was silicone oil or Ilfotol, no upstream disturbance was observed in our experiments because the suspending fluid was not disturbed sufficiently by the advancing bubble. It is worth noting that upstream disturbances have been observed to exist in silicone oils in thinner gaps (T. Maxworthy, personal communication), which again suggests that the upstream disturbance is a generic feature of bubble motion in a thin gap.

In order to account for the vigorous edge-jet structure, we must consider the influence of the redistribution of surfactant material by the surface velocity field associated with the rolling bubble surface. While the surfactant concentrations were not controlled or measured in our experiments, surfactants are generally present in all but the cleanest aqueous solutions. At the leading edge of the bubble (consider, for example, point N in figure 5), the emplacement of surface material onto the channel walls leads to a region of surface divergence, where the concentration of surfactant material must be decreased. At the trailing edge (for example, point T in figure 5), surface material is rolled off the glass plates, giving rise to an area of surface convergence and a local maximum in surfactant concentration on the trailing edge of the bubble. Surfactants act to decrease the local surface tension (Levich 1962); consequently, the surfactant concentration gradient along the edge of the bubble leads to an azimuthal surface tension gradient, or surface traction, which drives the edge jet.

We emphasize that the edge jet exists only by virtue of the three-dimensionality of the surface motion. If the flow around the bubble were purely two-dimensional, then (as in the analogous three-dimensional problem of flow past a spherical bubble) the advective redistribution of surfactant could only act to resist the surface flow and so to rigidify the bubble. The reversed surface flow observed in our thin-gap geometry relies explicitly on the generation of areas of intense surface divergence and convergence by the interaction of the bubble surface with the channel walls.

The physical picture presented here may be complicated by a number of effects neglected in our description. In particular, the channel walls may be dirty, and so may serve as a secondary source of surfactant material for the trailing edge. Such an effect would serve to amplify the tail-to-nose gradient in surface tension, and so too the associated edge jet. However, the radius of the wake separatrix did not change appreciably as the bubble advanced along the channel; moreover, the form of the flow accompanying successive bubbles released in turn (and so rising between progressively cleaner walls) did not change. These observations both indicate that the effect of surfactant material acquired from the channel walls was not dominant.

4. Governing equations

Consider a fluid of uniform density ρ and kinematic viscosity ν confined within a thin channel of thickness d. The bounding plates of the channel are inclined at a shallow angle α relative to the horizontal. We introduce a Cartesian coordinate system (x, y, z) such that x and y vary along, respectively, the width and the length of the channel, and $z = 0$ and $z = d$ define the upper and lower channel boundaries. A bubble of volume $V = \pi a^2 d$ and zero density is injected at the bottom of the channel ($z = 0$), and subsequently rises in the y-direction under the influence of gravity $g \sin\alpha$. The characteristic bubble size a is large relative to the gap width, $a/d \gg 1$.

Non-dimensionalizing the Navier–Stokes equations on the basis of a convective timescale a/U, velocity scale U, horizontal lengthscale a, cross-gap lengthscale d, and dynamic pressure scale P_0 yields the equations governing the motion in the suspending fluid:

$$\frac{\mathrm{D}\boldsymbol{u}}{\mathrm{D}t} = -\frac{P_0}{\rho U^2}\,\nabla p_d + \frac{\nu}{Ua}\frac{a^2}{d^2}\left(\frac{\partial^2 \boldsymbol{u}}{\partial z^2} + \frac{d^2}{a^2}\left(\frac{\partial^2 \boldsymbol{u}}{\partial x^2} + \frac{\partial^2 \boldsymbol{u}}{\partial y^2}\right)\right), \quad \nabla \cdot \boldsymbol{u} = 0, \tag{4.1}$$

where $p_d = (p - \rho g z \sin\theta)/P_0$ is the non-dimensional dynamic pressure. When the gap is thin, $(d/a)^2 \ll 1$, the relative magnitude of the inertial and viscous forces is given by the gap Reynolds number, $Re(d/a)^2$. When $Re(d/a)^2 \ll 1$, the inertial forces may be neglected and the flow is governed by Stokes equations. When $Re(d/a)^2 \gg 1$, viscous effects are confined to thin boundary layers adjoining the channel walls and bubble surface. The anomalous wake structure was observed for $1 < Re(d/a)^2 < 50$; consequently, both inertial and viscous forces will be significant (Riegels 1938).

The stress balance at the bubble surface assumes the form

$$(\boldsymbol{n} \cdot \boldsymbol{\tau} - \boldsymbol{n} \cdot \hat{\boldsymbol{\tau}}) = \sigma \boldsymbol{n} \nabla_s \cdot \boldsymbol{n} - \nabla_s \sigma$$

where $\boldsymbol{n}$ is the unit vector normal to the bubble surface, and $\nabla_s = (\boldsymbol{I} - \boldsymbol{nn}) \cdot \nabla$ is the surface gradient operator. The external and internal stress tensors are defined, respectively, through

$$\boldsymbol{\tau} = -(p_d + \rho g x)\,\boldsymbol{I} + 2\rho\nu\,\boldsymbol{E}, \quad \hat{\boldsymbol{\tau}} = -\hat{p}\boldsymbol{I}.$$

where $\boldsymbol{E}$ is the rate-of-strain tensor. The bubble shape is described by a balance between the normal stress jump across the bubble surface and the curvature force associated with the surface tension:

$$\boldsymbol{n} \cdot (\boldsymbol{n} \cdot \boldsymbol{\tau} - \boldsymbol{n} \cdot \hat{\boldsymbol{\tau}}) = \sigma \nabla_s \cdot \boldsymbol{n}. \tag{4.2}$$

The tangential stress balance takes the explicit form

$$\boldsymbol{t} \cdot (\boldsymbol{n} \cdot \boldsymbol{\tau} - \boldsymbol{n} \cdot \hat{\boldsymbol{\tau}}) = -\boldsymbol{t} \cdot \nabla_s \sigma \tag{4.3}$$

where $\boldsymbol{t}$ is the unit vector tangent to the bubble surface, and $\boldsymbol{t} \cdot \nabla_s \sigma$ represents tangential gradients in surface tension associated with gradients in surfactant concentration.

The surfactant concentration Γ on a bubble surface generally evolves according to

$$\frac{\partial \Gamma}{\partial t} + \nabla_s \cdot (\Gamma \boldsymbol{u}_s) + \Gamma (\nabla_s \cdot \boldsymbol{n})\,(\boldsymbol{u} \cdot \boldsymbol{n}) = J(\Gamma, C_s) + D_s \nabla_s^2 \Gamma \tag{4.4}$$

where $\boldsymbol{u}_s = (\boldsymbol{I} - \boldsymbol{nn}) \cdot \boldsymbol{u}$ is the surface velocity field, and D_s the surface diffusivity of surfactant material (e.g. Stone 1990). $J(\Gamma, C_s)$ represents a surfactant source term associated with adsorption onto or desorption from the bubble surface whose magnitude depends on the concentration of surfactant in the bulk, C_s, as well as the local surface concentration. Since the bubble is not changing shape to leading order, the

third term, which represents the change in surfactant concentration due to bubble expansion, may be neglected. The effects of surface diffusivity are typically negligible. Moreover, if we assume that the surfactant is insoluble, we can neglect the transport of surfactant to and from the bulk so that $J = 0$. Thus (4.4) indicates that a steady-state surfactant concentration may be maintained by a surface velocity field which satisfies

$$\Gamma(\nabla_s \cdot \boldsymbol{u}_s) + \boldsymbol{u}_s \cdot \nabla_s \Gamma = 0. \tag{4.5}$$

Inhomogeneities in surfactant concentration may thus be generated by regions of non-zero surface divergence on the bubble surface, such as those at the leading and trailing edges of the rolling bubble.

5. Theoretical model

A complete theoretical treatment of the problem would require coupling the surfactant transport equation to the dynamics of the external flow. In particular, it would be necessary to deduce a surface tension distribution which is consistent with both the external flow and the surfactant distribution on the bubble surface. While it is possible to develop a simple model of surfactant transport along the bubble surface on the basis of (4.5), it is not possible to link the surfactant distribution to the surface tension distribution without knowledge of the functional form of $\sigma(\Gamma)$. In the absence of this functional form, we consider the relatively simple kinematic problem of the motion of a bubble with a prescribed non-uniform surface tension distribution.

We have seen that the three-dimensionality of the surface flow plays a vital role in driving the anomalous wake structure; in particular, it is responsible for the redistribution of surfactants and so for establishing the tail-to-nose surface tension gradient. In developing theoretical models, we assume that the net effect of the three-dimensionality of the flow is to generate a two-dimensional nose-to-tail surface tension gradient along the bubble surface, and that the resulting flow is confined to lie in horizontal planes. We note that this assumption of two-dimensionality in the suspending fluid is expected to break down in the vicinity of the bubble, where three-dimensional corner flows (of the form responsible for the upstream disturbance arising in the absence of surfactants) are expected to arise. Finally, we have seen that the anomalous wake structure arises in the moderate-Reynolds-number regime, which does not lend itself to straightforward analysis. In Appendices A and B, we consider two highly idealized models of Marangoni bubble motion, respectively high- and low-*Re* flow past a two-dimensional circular bubble with an applied surface stress. In what follows, we develop a model which incorporates the relevant bounding geometry and allows a three-dimensional flow structure. We assume for the sake of simplicity that the gap Reynolds number is small, in which case (4.1) indicates that the fluid motion is governed by the Stokes equations, so that the thin gap corresponds to a Hele-Shaw cell (Riegels 1938).

We consider the uniform translation of a buoyant bubble corresponding to a flat circular cylinder of radius a and thickness d with a prescribed non-uniform surface tension. We adopt cylindrical polar coordinates, (r, θ, z), where $r = 0$ defines the bubble's centre, and the bounding walls again correspond to $z = 0$ and $= d$. We assume that the surface tension distribution takes the form

$$\sigma(\theta) = \sigma_0 + a\gamma \cos\theta, \tag{5.1}$$

where $\theta = 0$ corresponds to the nose of the bubble, and γ denotes the magnitude of

the gradient in surface tension, or equivalently the applied surface stress. While other possibilities exist for $\sigma(\theta)$, the chosen cosinusoidal dependence is consistent with the proposed physical picture, since one expects the surface divergence associated with the rolling bubble to vary as $\hat{\boldsymbol{y}} \cdot \hat{\boldsymbol{r}}$ along the bubble surface.

The boundary conditions assume the explicit form

$$u_r = 0 \text{ at } r = a \tag{5.2}$$

$$\boldsymbol{u} \to -U\hat{\boldsymbol{y}} \text{ as } r \to \infty, \tag{5.3}$$

and the tangential stress balance (4.3) takes the form

$$\mu \frac{\partial}{\partial r}\left(\frac{u_\theta}{r}\right) = \gamma \sin\theta. \tag{5.4}$$

In treating problems involving drop and bubble motion in a Hele-Shaw cell, it is common to assume that the velocity field has a separable form:

$$\boldsymbol{u}(r, \theta, z) = \boldsymbol{v}(r, \theta)\frac{6(zd - z^2)}{d^2}, \tag{5.5}$$

where $\boldsymbol{v}(r, \theta)$ represents a depth-averaged velocity within the gap, and the cross-gap z-dependence corresponds to that of Poiseuille flow. Substituting (5.5) into Stokes equations yields Brinkmann's equations which describe the two-dimensional velocity field

$$\nabla p = \mu\left(\nabla^2 - \frac{k^2}{a^2}\right)\boldsymbol{v}, \quad \nabla \cdot \boldsymbol{v} = 0, \tag{5.6}$$

where $k^2 = 12a^2/d^2$ indicates the aspect ratio of the bubble, and ∇ now corresponds to the horizontal gradient operator. The Darcy flow equation, which is typically used to describe bubble motion in a Hele-Shaw cell, is recovered from (5.6) by omitting the $\nabla^2\boldsymbol{v}$ term; however, this term must be retained here in order to account for the influence of the applied surface stress (Boos & Thess 1997).

We must solve (5.6) for the depth-averaged velocity $\boldsymbol{v}$ subject to boundary conditions (5.2)–(5.4). We express the velocity field in terms of a streamfunction Ψ:

$$\boldsymbol{v} = \nabla \wedge (\Psi\hat{\boldsymbol{z}}) = \left(\frac{1}{r}\frac{\partial \Psi}{\partial \theta}, -\frac{\partial \Psi}{\partial r}\right). \tag{5.7}$$

According to (5.6), Ψ must satisfy

$$\nabla^2\left(\nabla^2 - \frac{k^2}{a^2}\right)\Psi = 0. \tag{5.8}$$

Since Brinkmann's equations are linear, we may deduce the desired solution by decomposing the problem into two simpler component parts. Specifically, we solve for the flow associated with a bubble rising in a thin gap, which satisfies boundary conditions (5.2)–(5.3) but not (5.4), and superpose the solution for the flow driven by a surface traction on a stationary bubble. We thus write $\Psi = \Psi_s + \Psi_m$, where Ψ_s is the streamfunction associated with the bubble's uniform translation, and Ψ_m is the Marangoni component associated with the applied surface traction.

The solution for the streamfunction Ψ_s may be deduced by noting that the solution for Darcy flow around a two-dimensional circle is also a solution of (5.8). Consequently, Ψ_s simply corresponds to the streamfunction describing inviscid flow past

a rising circle, or, equivalently, that around a translating dipole of dipole moment $M = Ua^2$:

$$\Psi_s = Ua \left(\frac{1}{r'} - r'\right) \sin\theta, \tag{5.9}$$

where $r' = r/a$. This flow makes a contribution $-2(\mu U/a)\sin\theta$ to the tangential stress at the bubble surface. Consequently, we must seek a solution Ψ_m corresponding to the flow around a stationary bubble with a prescribed surface stress

$$\tau_{r\theta} = \left(\gamma + 2\,\frac{\mu U}{a}\right) \sin\theta. \tag{5.10}$$

The problem of the Marangoni flow induced by a bubble of arbitrary shape and fixed in a Hele-Shaw cell in the presence of a horizontal temperature gradient has been treated by Boos & Thess (1997), whose solution for a circular bubble may be readily adapted to our problem. Solving (5.8) subject to boundary conditions (5.2), (5.10) and $\boldsymbol{v} \to 0$ as $r \to \infty$ yields a streamfunction which can be expressed in terms of the modified Bessel functions of the first and second kind, I_n and K_n, through

$$\Psi_m = Ua\,(T+2)\sin\theta \frac{I_2(k)K_1(k)}{k^2K_1(k) + 2kI_2(k)K_0(k)} \left(\frac{K_1(kr')}{K_1(k)} - \frac{1}{r'}\right), \tag{5.11}$$

where T prescribes the relative magnitudes of the applied surface stress and the characteristic viscous stress in the problem,

$$T = \frac{\gamma}{\mu U/a} = \frac{\text{surface stress}}{\text{viscous stress}}, \tag{5.12}$$

and so corresponds to the inverse of a dynamic capillary number. In the limit of a very flat bubble, $k \to \infty$, (5.11) reduces to the form

$$\Psi_m \;=\; Ua\,(T+2)\,\frac{1}{k^2}\left(\frac{1}{r'} \;-\; \exp(k(1-r'))\right)\sin\theta. \tag{5.13}$$

The full solution for the streamfunction $\Psi = \Psi_s + \Psi_m$ is deduced by superposing (5.9) and (5.13). The associated velocity field, calculated from (5.7), is given by

$$\frac{v_r}{U\cos\theta} = -1 + \frac{a^2}{r^2} + \frac{T+2}{k^2}\,\frac{a^2}{r^2} - \frac{T+2}{k^2}\,\frac{1}{r'}\,\exp(k(1-r')), \tag{5.14}$$

$$\frac{v_\theta}{U\sin\theta} = \underbrace{1}_{\text{free stream}} + \underbrace{\frac{a^2}{r^2}}_{\text{dipole}} + \underbrace{\frac{T+2}{k^2}\,\frac{a^2}{r^2}}_{\text{anomalous dipole}} - \underbrace{\frac{T+2}{k^2}\,k\,\exp(k(1-r'))}_{\text{boundary layer}}. \tag{5.15}$$

The flow is characterized by two distinct regions: a boundary layer adjoining the bubble surface and a potential flow exterior. The boundary layer is required in order to satisfy the tangential stress condition at the bubble surface, and has a thickness of $O(a/k)$ comparable to the gap width. The azimuthal boundary-layer velocity is large, $O(k)$, relative to the translation speed, and the associated boundary-layer flux, obtained by integrating the final term in (5.15) from $r = a$ to ∞, is given by

$$F_\theta(\theta) = -U\,a^2\,\frac{T+2}{k^2}\,\sin\theta. \tag{5.16}$$

In our problem, the surface tension is highest at the leading edge ($T > 0$); consequently, the boundary-layer flux is always towards the nose of the bubble, and so opposes the free stream.

The surface velocity field takes the form

$$v_\theta(a,\theta) = \left(2 - (T+2)\frac{k-1}{k^2}\right)\sin\theta. \tag{5.17}$$

The applied surface stress clearly serves to reduce the surface velocity. Moreover, in the large-k limit under consideration, the surface velocity will reverse when $T > 2k$: the thinner the gap, the greater the surface stress required to reverse the surface flow. Surface flow reversal thus requires that, in dimensional terms,

$$\gamma > \sqrt{12}\,\frac{\mu U}{d}, \tag{5.18}$$

so that the applied surface stress exceeds the viscous stress resisting flow in the thin gap.

For $T < 2k$, the flow past the bubble is weakly disturbed by the applied surface stress. No surface velocity reversal occurs, and no bounding streamline exists. For $T > 2k$, however, surface reversal occurs and (5.14) indicates that the radial velocity vanishes not only on the bubble surface, $r = a$, but also on a separatrix of radius

$$R = a\left(1 + \frac{T+2}{k^2}\right)^{1/2}. \tag{5.19}$$

The flow outside the boundary layer corresponds to the potential flow associated with a dipole with moment of magnitude $M = UR^2$ translating with speed U. The anomalous dipole moment $Ua^2(T+2)/k^2 = U(R^2 - a^2)$ identified in (5.14)–(5.15) is supported by the boundary-layer transport (5.16) associated with the applied surface stress. Increasing the aspect ratio k of the bubble serves to reduce the radius of the encircling wake; conversely, increasing T serves to increase the boundary-layer transport, and so too the anomalous dipole moment of the bubble.

Figure 9 illustrates the fluid streamlines for the case $T > 2k$, and clearly illustrates the presence of an encircling wake and an intense boundary layer flow, or 'edge jet' adjoining the bubble surface. This theoretically predicted flow bears a striking resemblance to that observed in the laboratory and illustrated in figures 1 and 2.

On the basis of this model, we may deduce the rise speed of a bubble through an inclined Hele-Shaw cell in the presence of an applied surface stress. The local dissipation rate per unit area for Poiseuille flow is

$$\Phi = \frac{12\mu(v_r^2 + v_\theta^2)}{d}. \tag{5.20}$$

Consequently, the total dissipation rate Φ_T may be obtained by substituting the velocity field (5.14)–(5.15) (less the free stream) into (5.20), and integrating over the entirety of the suspending fluid:

$$\Phi_T = 2\int_0^\pi \int_a^\infty \Phi r\,\mathrm{d}r\;\mathrm{d}\theta. \tag{5.21}$$

It can be shown via (5.14)–(5.15) that the viscous dissipation associated with the boundary-layer flow is small, $O(k^{-3})$, relative to that associated with the potential flow when $R > a$. To leading order, the total dissipation rate is thus that associated

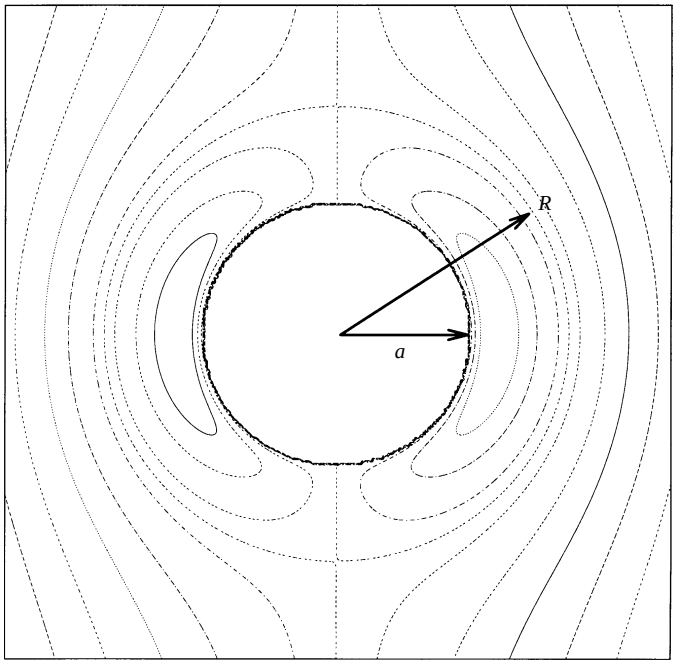

FIGURE 9. The theoretically predicted streamlines, in the bubble frame of reference, indicating the flow around a bubble rising in a Hele-Shaw cell subject to a surface traction, with $k = 10, T = 200$. Note the separatrix of radius $R = 1.74a$, and the intense boundary-layer motions adjoining the bubble surface and characterized by a reversed surface flow.

with the dipolar potential flow, which is given by

$$\Phi_T = 12\pi\mu U^2 R^2 \frac{1}{d}, \tag{5.22}$$

and so is identical to that associated with a circular bubble of radius R translating at speed U. Equating the total viscous dissipation in the system with the rate of work done by buoyancy,

$$12\pi\mu U^2 R^2 \frac{1}{d} = \pi a^2 d U \rho g \sin\alpha, \tag{5.23}$$

yields a steady rise speed

$$U = U_0 \frac{a^2}{R^2}, \quad \text{where} \quad U_0 = \frac{g\, d^2}{12\, \nu} \sin\alpha \tag{5.24}$$

is the rise speed of a bubble in a Hele-Shaw cell deduced by neglecting the tangential stress condition on the bubble surface (Maxworthy 1986). The effect of the surface forcing enters uniquely through the dependence on the radius of the encircling wake. As the applied surface stress increases, so too does the anomalous dipole moment, and the viscous dissipation in the system. Consequently, as the radius of the encircling wake increases, the bubble rise speed decreases.

Finally, when $T = 0$, (5.24) and (5.19) yield the rise speed of a flat ($k \gg 1$) circular bubble in a Hele-Shaw cell in the absence of an applied surface stress:

$$U = U_0 \left(1 - \frac{2}{k^2}\right). \tag{5.25}$$

Nadim *et al.* (1996) computed the leading order, $O(k^{-1})$, correction to the rise speed of a circular drop in a Hele-Shaw cell required by application of the tangential stress boundary conditions at the drop surface, and found that this correction vanishes in the limit of zero drop viscosity. Consequently, (5.25) represents the leading-order correction to the rise speed of a flat circular bubble in a Hele-Shaw cell associated with application of the zero tangential stress boundary condition at the bubble surface.

6. Discussion

Our theoretical model of Marangoni bubble motion in a Hele-Shaw cell predicts a flow whose form is strikingly similar to that observed in the laboratory. While the Hele-Shaw description is not directly relevant to the observed moderate-Reynolds-number flow, it is interesting to see what inferences can be made from the model concerning the magnitude of the surface tension gradient generated on the bubble surface in the laboratory.

In our experimental study, at the lowest observed gap Reynolds number, $Re(d/a)^2 \sim 1$, the wake was circular, with a radius $R/a \sim 1.3$. The bubble aspect ratio was typically $k = \sqrt{12}\,a/d \sim 50$, and the rise speed $U \sim 0.5$ cm s^{-1}. According to our result (5.19) for the radius of the separatrix, this implies a nose-to-tail change in surface tension in our experiments of order

$$\frac{\Delta\sigma}{\sigma} \sim k^2 \left(\frac{R^2}{a^2} - 1\right) \mu U \frac{1}{\sigma} \sim 20\% , \tag{6.1}$$

which is a change characteristic of those induced by surfactants in air–water systems. Substituting the bubble rise speed (5.24) into the criterion (5.18) for surface flow reversal indicates that an encircling wake will exist only when

$$\gamma > \frac{2}{k}\rho g a \sin\alpha, \tag{6.2}$$

and so is dependent on the gravitational pressure change across the bubble being sufficiently small. Indeed, we were able to observe this anomalous wake structure in the laboratory only because the tilted channel represents an experimental analogue of a reduced-gravity environment (Eck & Siekmann 1978).

Surface tension gradients associated with the mechanical redistribution of surfactant material are important in a number of problems, for example in the forced wetting of fibres (Quéré, de Ryck & Ramdane 1997) and in the motion of gas bubbles in capillary tubes (Ratulowski & Chang 1990). In our experiments, the gradient in surface tension at the bubble surface is generated mechanically by the surface motions associated with the bubble advancing in the thin-gap geometry. There are also a number of physical situations where analogous (nose-to-tail) surface tension gradients may be produced by an external forcing, in particular by a gradient in either temperature or surfactant concentration in the suspending fluid. Since surface tension decreases with both temperature and surfactant concentration, nose-to-tail surface tension gradients will accompany bubbles rising along an adverse temperature or surfactant gradient.

Young, Goldstein & Block (1959) examined low-*Re* bubbles rising in a temperature gradient and predicted that at a critical temperature gradient, the buoyancy-driven motion will halt. Their accompanying experimental study verified this prediction, and demonstrated that for temperature gradients in excess of a critical value, the bubbles migrate downwards towards the heat source. While the possibility of an encircling wake or separatrix accompanying thermocapillary bubble motion was not

identified by Young *et al.* (1959), it has been clearly illustrated by Merrit, Morton & Subramanian (1993). Finally, Rednikov, Ryazantsev & Velarde (1994) considered the steady low-*Re* translation of a droplet through a surfactant-rich suspending fluid, and examined the effects of a chemical reaction on the drop surface which decreases the local surfactant concentration. A reversed surface flow and heightened drag associated with a fore-aft-symmetric recirculating wake were predicted to exist in certain parameter regimes. It is worth noting that much of the analysis developed for describing thermocapillary drop motion in microgravity may be readily applied in describing various aspects of the flow reported here.

Stebe, Lin & Maldarelli (1990) considered the motion of air slugs along a cylindrical capillary tube, and demonstrated that the ability of surfactants to generate surface stresses and so to resist surface flow vanishes when the concentration of surfactant in the suspending fluid is sufficiently high. In this case, the diffusion of the surfactant material from the suspending fluid can occur sufficiently rapidly to suppress surface gradients in surfactant concentration and so act to remobilize the surface. This physical effect accounts for our observation that the addition of soap or surfactant to the suspending fluid may serve to reduce the vigour of the reversed flow. When the suspending fluid is concentrated surfactant, it is impossible to establish surface gradients in surfactant concentration, and the edge jet is completely suppressed.

The edge jet was also observed to vanish when the suspending fluid was silicone oil since surfactants are generally inactive in silicone–air systems (Park *et al.* 1994). Finally, the anomalous wake structure (specifically, the edge jet) was most pronounced when the suspending fluid was saltwater. This observation is in accordance with those of Scott (1975), who demonstrated that small air bubbles are less likely to coalesce in saltwater than in pure water, and ascribed this effect to the increased elasticity imparted to the bubble surfaces by the heightened influence of surfactants in the saltwater solutions.

7. Conclusions

We have reported a novel flow structure observed to accompany bubbles rising through a thin gap of liquid, which represents an example of a mechanically forced Marangoni flow. The flow is characterized by an intense reversed surface flow and an encircling wake defined by a bounding streamline. Details of the flow structure, and the form of its evolution with increasing Reynolds number have been outlined through a series of experiments. The vigour of the anomalous wake structure was observed to depend critically on the suspending fluid, with the edge jet being entirely absent in silicone oil and Ilfotol, present in all aqueous solutions, and most pronounced in saltwater solutions. These observations may be accounted for by the relative impact of surfactants in each case.

The anomalous wake structure may be understood by noting that the surfactants serve to impart an effective elasticity to the bubble surface. The form of the observed surface flow may thus be understood by imagining the motion of an elastic balloon rolling upwards between two plates if one assumes that the balloon surface must adhere to the bounding plates as it advances. In this case, the surface tension of the balloon will be large along its leading edge as the balloon material is rolled onto the bounding plates. Conversely, the trailing edge will go slack due to the material being rolled off the bounding walls. In reality, the balloon may burst due to the large tensions generated at its leading edge; however, if it were sufficiently elastic and its surface sufficiently mobile, one could imagine a surface motion similar to that

illustrated in figure 5. In particular, one would expect the gradient in surface tension along the balloon's edge to draw surface material from the rear to the nose of the balloon.

Surfactants thus play an anomalous role in the flow reported here. While their usual role in the dynamics of bubbles is to immobilize surfaces and so to reduce the magnitude of the surface velocity, they here serve to generate vigorous reversed flow on the bubble surface. The vertical momentum associated with the reversed surface motions contributes significantly to the hydrodynamic drag on the bubble. Moreover, through generating a circular wake with a bounding separatrix, surfactants significantly alter the transport properties of the rising bubble.

A theoretical model of Marangoni bubble motion in a Hele-Shaw cell was developed which reproduced the salient features of the observed wake structure. It is worth noting that the analysis presented in §5, while developed in order to describe the mechanically forced Marangoni flow reported here, applies equally well in describing Marangoni bubble motion in a Hele-Shaw cell in the presence of an externally imposed gradient in either temperature or surfactant.

The author gratefully acknowledges financial support through an NSERC of Canada Postdoctoral Fellowship. The author thanks Oliver Jensen, John Lister, Howard Stone and Tony Maxworthy for many valuable discussions and for their comments on the manuscript, Stuart Dalziel for a number of helpful suggestions concerning the experiments and for his assistance with the particle-tracking, Ian Eames, John Harper and Manuel Velarde for a number of useful discussions, and Paul Linden for generously granting him access to the DAMTP laboratory facilities.

Appendix A. High-*Re* flow past a circular bubble with an applied surface stress

We consider the case of high-*Re* flow past a circular bubble with a prescribed surface stress of the form (5.1) by adapting Moore's (1965) analysis of high-*Re* flow past a spherical bubble. Our problem differs from that of Moore in that we consider a two-dimensional geometry, and the flow must satisfy a non-zero tangential stress condition at the bubble surface associated with the applied stress. We express the flow as a superposition of inviscid flow past a circle, $\bar{\boldsymbol{u}}(\boldsymbol{x})$, and a perturbation flow $\boldsymbol{u}'(\boldsymbol{x})$ required to satisfy the tangential stress boundary condition (5.4) on the bubble surface:

$$\boldsymbol{u}(\boldsymbol{x}) = \bar{\boldsymbol{u}}(\boldsymbol{x}) + \boldsymbol{u}'(\boldsymbol{x}). \tag{A 1}$$

We substitute the flow field (A 1) into the Navier–Stokes equations in two-dimensional polar coordinates in order to obtain the relevant boundary-layer equations. We drop the primes on the boundary-layer flow components and so obtain

$$\frac{1}{r}\frac{\partial}{\partial r}(ru_r) + \frac{1}{r}\frac{\partial u_\theta}{\partial \theta} = 0, \tag{A 2}$$

$$\bar{u}_r\,\frac{\partial u_r}{\partial r} + \frac{\bar{u}_\theta}{r}\,\frac{\partial u_r}{\partial \theta} + u_r\frac{\partial \bar{u}_r}{\partial r} + \frac{u_\theta}{r}\frac{\partial \bar{u}_r}{\partial \theta} - \frac{2}{r}\bar{u}_\theta u_\theta - \frac{u_\theta^2}{r} = -\frac{1}{\rho}\frac{\partial p}{\partial r} + \nu\left(\nabla^2 u_r - \frac{u_r}{r^2} + \frac{2}{r^2}\frac{\partial u_\theta}{\partial \theta}\right), \tag{A 3}$$

$$\bar{u}_r\frac{\partial u_\theta}{\partial r} + \frac{\bar{u}_\theta}{r}\frac{\partial u_\theta}{\partial \theta} + u_r\frac{\partial \bar{u}_\theta}{\partial r} + \frac{u_\theta}{r}\frac{\partial \bar{u}_\theta}{\partial \theta} + \frac{\bar{u}_r u_\theta}{r} + \frac{u_r\bar{u}_\theta}{r} = -\frac{1}{\rho r}\frac{\partial p}{\partial \theta} + \nu\left(\nabla^2 u_\theta - \frac{u_\theta}{r^2} + \frac{2}{r^2}\frac{\partial u_r}{\partial \theta}\right), \tag{A 4}$$

where the barred quantities are the solutions for inviscid flow past a circle:

$$\bar{u}_r = U\left(\frac{a^2}{r^2} - 1\right)\cos\theta, \quad \bar{u}_\theta = U\left(\frac{a^2}{r^2} + 1\right)\sin\theta. \tag{A 5}$$

The boundary-layer variables must satisfy the boundary conditions

$$u_r = 0 \text{ on } r = a, \text{ and } u_r \to 0 \text{ as } r \to \infty, \tag{A 6}$$

$$u_\theta = 0 \text{ at } \theta = 0, \text{ and } u_\theta \to 0 \text{ as } r \to \infty, \tag{A 7}$$

and the tangential stress balance at the bubble surface takes the form

$$\frac{\partial u_\theta}{\partial r} = \left(\frac{4U}{a} + \frac{2\gamma}{\mu}\right)\sin\theta. \tag{A 8}$$

We assume that the second term on the right-hand side does not exceed the third, in which case the boundary-layer variables remain small relative to the barred quantities. In this case, the analysis of Moore (1965) may be followed.

Since continuity requires that $\bar{u}_\theta = O(1)$ and $\bar{u}_r = O(Re^{-1/2})$ in the boundary layer, equations (A 2)–(A 4) and (A 8) suggest the following scalings for the boundary layer variables:

$$u_\theta = O(Re^{-1/2}),\ u_r = O(Re^{-1}),\ p = O(Re^{-1}). \tag{A 9}$$

Consequently, the leading order, $O(Re^{-1/2})$, terms in (A 4) are

$$\bar{u}_r\frac{\partial u_\theta}{\partial r} + \frac{\bar{u}_\theta}{r}\frac{\partial u_\theta}{\partial \theta} + \frac{u_\theta}{r}\frac{\partial \bar{u}_\theta}{\partial \theta} = \frac{\partial^2 u_\theta}{\partial r^2}. \tag{A 10}$$

We introduce a non-dimensional azimuthal velocity $u = (u_\theta/U)\,Re^{1/2}$ and a stretched boundary-layer coordinate $y = Re^{1/2}(r/a - 1)$. Substituting into (A10) thus yields an equation for $u(y)$ of the form

$$2\frac{\partial}{\partial\theta}(u\sin\theta) - 2y\cos\theta\frac{\partial u}{\partial y} = \frac{\partial^2 u}{\partial y^2} \tag{A 11}$$

which must be solved subject to the non-dimensionalised boundary conditions:

$$u = 0 \text{ at } \theta = 0,\ u \to 0 \text{ as } r \to \infty, \tag{A 12}$$

$$\frac{\partial u}{\partial y} = (4 + T)\sin\theta \text{ at } y = 0, \tag{A 13}$$

where T is the surface stress parameter defined in (5.12). We seek a solution of the form

$$u = \sin\theta\ X^{1/2}(\theta)\ f(t) \tag{A 14}$$

where $t = y/(2X^{1/2})$, so that $X^{1/2}(\theta)$ is an equivalent boundary-layer thickness. This solution form yields solutions provided $X(\theta)$ takes the form

$$X(\theta) = \tfrac{1}{2}\,\mathrm{cosec}^4\theta\left(\tfrac{2}{3} - \cos\theta + \tfrac{1}{3}\cos^3\theta\right), \tag{A 15}$$

in which case (A 11) reduces to the form

$$\frac{\mathrm{d}^2 f}{\mathrm{d}t^2} + 2t\frac{\mathrm{d}f}{\mathrm{d}t} - 2f = 0. \tag{A 16}$$

By inspection, one solution is $f(t) = 2t$. The other linearly independent solution may be obtained by reduction of order, and is given by

$$f(t) = \pi^{-1/2}\,\mathrm{e}^{-t^2} - t\,\mathrm{erfc}(t) \tag{A 17}$$

where erfc(t) is the complementary error function. The general solution for the perturbation to the azimuthal component of the flow required by the applied tangential stress at the bubble surface is thus given by

$$u'_\theta(r,\theta) = -2\ Re^{-1/2}\ U(4+T)\ \sin\theta\ X^{1/2}(\theta)\ f(t). \tag{A 18}$$

The flow is thus uniquely prescribed by two non-dimensional groups, namely Re and T.

The surface velocity takes the form

$$u_\theta(a,\theta) = 2U\ \sin\theta\left(1 - Re^{-1/2}(4+T)X(\theta)\right) \tag{A 19}$$

The boundary-layer disturbance is by assumption small in our analysis; consequently, it is not possible to examine the large-T regime in which the surface flow reverses. Nonetheless, (A 19) clearly indicates that the presence of the surface stress will retard the surface velocity, and suggests that surface velocity reversal will arise when $T \sim Re^{1/2}$.

Appendix B. Stokes flow past a buoyant circular bubble with an applied surface stress

We here consider a buoyant circular bubble with a surface tension distribution (5.1) rising through a high-viscosity fluid. We solve the Stokes equations

$$-\nabla p_d = \mu\nabla^2\boldsymbol{u}, \quad \nabla\cdot\boldsymbol{u} = 0 \tag{B 1}$$

in two dimensions, subject to boundary conditions (5.2)–(5.4). The solution may be found by standard methods and assumes the form

$$\frac{u_r(r,\theta)}{U} = \frac{G}{4}\cos\theta\left((S\ -\ 1)\ \ln\ r' + S(1-r'^{-2})\right), \tag{B 2}$$

$$\frac{u_\theta(r,\theta)}{U} = \frac{G}{4}\sin\theta\left((1-S)(1+\ln r') - S(1+r'^{-2})\right), \tag{B 3}$$

where

$$G = \frac{\rho g a}{\mu U/a} = \frac{\text{gravitational pressure}}{\text{viscous stress}},$$

$$S = \frac{\gamma}{\rho g a} = \frac{\text{surface traction}}{\text{gravitational pressure}},$$

and $r' = r/a$. As in the case of Stokes flow past a rigid cylinder, a logarithmic term arises, making it impossible to satisfy the far-field boundary condition (5.3), and so to deduce the rise speed of the cylinder. Nonetheless, the solution is valid in the near-field region ($r < a/Re$), beyond which it must be fitted to Oseen's solution.

We are concerned with the flow in the vicinity of the circular bubble, and specifically with the possibility of an encircling wake. Equation (B 2) indicates that $u_r = 0$ at $r = a$ and at a second radius R defined by

$$S = \frac{R^2\ \ln(R/a)}{R^2 - a^2 + R^2\ \ln(R/a)}. \tag{B 4}$$

Real roots $R > a$ exist for $1/3 < S < 1$. According to (B 3), the surface velocity takes the explicit form

$$\frac{u_\theta(a,\theta)}{U} = \frac{G}{4}\ \sin\theta(1-3S).$$

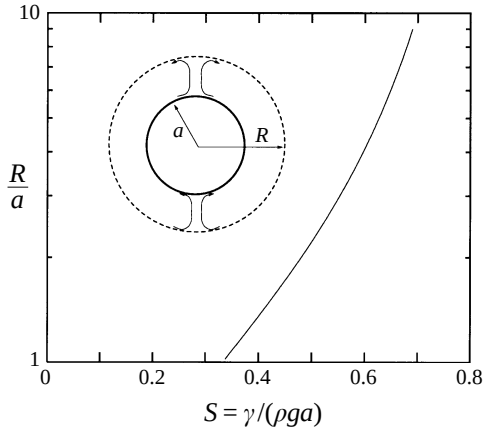

FIGURE 10. The predicted non-dimensional radius R/a of the wake encircling a two-dimensional bubble with an applied surface traction γ, and rising due to gravity through a high-viscosity fluid.

For $S < 1/3$, the surface traction acts to retard the surface flow, but is not of sufficient magnitude to reverse it. At the critical value $S = 1/3$, the surface flow vanishes identically, and for $S > 1/3$ a reversed surface flow must obtain. As indicated in figure 10, the radius of the encircling wake increases monotonically with S. At $S = 1$, the net force on the bubble is zero: the buoyancy force causing motion is precisely balanced by the downward reaction force associated with the surface traction imparting vertical momentum to the suspending fluid.

While this two-dimensional Stokes flow model is admittedly a very crude description of the observed three-dimensional moderate-Reynolds-number flow phenomenon, it does reproduce its most salient features, namely a bounding streamline encircling the bubble and a reversed surface flow.

REFERENCES

BOOS, W. & THESS, A. 1997 Thermocapillary flow in a Hele-Shaw cell. *J. Fluid Mech.* **352**, 305–330.

BUSH, J. W. M. & EAMES, I. 1998 Fluid displacement by high Reynolds number bubble motion in a thin gap. *Intl J. Multiphase Flow*, in press.

DALZIEL, S. B. 1992 Decay of rotating turbulence: some particle tracking experiments. *Appl. Sci. Res.* **49**, 217–244.

DUSSAN, V., E. B. 1977 Immiscible liquid displacement in a capillary tube: the moving contact line. *AIChE J.* **23**, 131–133.

ECK, W. & SIEKMANN, J. 1978 On bubble motion in a Hele-Shaw cell, a possibility to study two-phase flows under reduced gravity. *Ing. Archiv.* **47**, 153–168.

HARPER, J. F. 1972 The motion of bubbles and drops through liquids. *Adv. Appl. Mech.* **12**, 59–129.

LEVICH, V. G. 1962 *Physicochemical Hydrodynamics.* Prentice-Hall.

MAXWORTHY, T. 1986 Bubble formation, motion and interaction in a Hele-Shaw cell. *J. Fluid Mech.* **173**, 95–114.

MERRIT, R. M., MORTON, D. S. & SUBRAMANIAN, R. S. 1993 Flow structures in bubble migration under the combined action of buoyancy and capillarity. *J. Colloid Interface Sci.* **155**, 200–209.

MOORE, D. W. 1965 The velocity of rise of distorted gas bubbles in a liquid of small viscosity. *J. Fluid Mech.* **23**, 749–765.

NADIM, A., BORHAN, A. & HAJ-HARIRI, H. 1996 Tangential-stress and Marangoni effects at a fluid-fluid interface in a Hele-Shaw cell. *J. Colloid Interface Sci.* **181**, 159–164.

PARK, C.-W., MARUVADA, S. R. K. & YOON, D.-Y. 1994. The influence of surfactant on the bubble motion in Hele-Shaw cells. *Phys. Fluids* **6**, 3267–3275.

Quéré, D., Ryck, A. de & Rumdane, O. O. 1997 Liquid coating from a surfactant solution. *Europhys. Lett*. **37**, 305–310.

Ratulowski, J. & Chang, H.-C. 1990. Marangoni effects of trace impurities on the motion of long gas bubbles in capillaries. *J. Fluid Mech*. **210**, 303–328.

Rednikov, A. Y., Ryazantsev, Y. S. & Velarde, M. G. 1994 Drop motion with surfactant transfer in a homogeneous surrounding. *Phys. Fluids* **6**, 451–468.

Riegels, F. 1938 Zur Kritik des Hele-Shaw-Versuchs. *Z. Angew. Math. Mech*. **18**, 95.

Scott, J. C. 1975 The preparation of water for surface-clean fluid mechanics. *J. Fluid Mech*. **69**, 339–352.

Siekmann, J., Eck, W. & Johann, W. 1974 Experimentelle Untersuchungen uber das Verhalten von Gasblasen in einem Null-g-Simulator. *Z. Flugwiss*. **22**, 83–92.

Stebe, K. J., Lin S.-H. & Maldarelli, C. 1990 Remobilizing surfactant retarded particle interfaces. I. Stress-free conditions at the interfaces of micellar solutions of surfactants with fast sorption kinetics. *Phys. Fluids* A **3**, 3–20.

Stone, H. A. 1990 A simple derivation of the time-dependent convective-diffusion equation for surfactant transport along a deforming interface. *Phys. Fluids* A **2**, 111–112.

Young, N. O., Goldstein, J. S. & Block, M. J. 1959. The motion of bubbles in a vertical temperature gradient. *J. Fluid Mech*. **5**, 350–356.